From Half-Metal to Semiconductor: Electron-Correlation Effects in Zigzag SiC Nanoribbons From First Principles

Naresh Alaal,[1,2,3] Vaideesh Loganathan,[2] Nikhil Medhekar,[3] and Alok Shukla[2,*]

[1]*IITB-Monash Research Academy, Indian Institute of Technology Bombay, Powai, Mumbai 400076, India*
[2]*Department of Physics, Indian Institute of Technology Bombay, Mumbai 400076, India*
[3]*Department of Materials Engineering, Monash University, Clayton, Victoria 3800, Australia*

(Received 25 November 2016; revised manuscript received 19 April 2017; published 9 June 2017)

We perform electronic-structure calculations based on the first-principles many-body–theory approach in order to study quasiparticle band gaps and optical absorption spectra of hydrogen-passivated zigzag SiC nanoribbons. Self-energy corrections are included using the *GW* approximation, and excitonic effects are included using the Bethe-Salpeter equation. We systematically study nanoribbons that have widths between 0.6 and 2.2 nm. Quasiparticle corrections widen the Kohn-Sham band gaps because of enhanced interaction effects, caused by reduced dimensionality. Zigzag SiC nanoribbons with widths larger than 1 nm exhibit half-metallicity at the mean-field level. The self-energy corrections increase band gaps substantially, thereby transforming the half-metallic zigzag SiC nanoribbons to narrow gap spin-polarized semiconductors. Optical absorption spectra of these nanoribbons get dramatically modified upon inclusion of electron-hole interactions, and the narrowest ribbon exhibits strongly bound excitons, with binding energy of 2.1 eV. Thus, the narrowest zigzag SiC nanoribbon has the potential to be used in optoelectronic devices operating in the IR region of the spectrum, while the broader ones, exhibiting spin polarization, can be utilized in spintronic applications.

DOI: 10.1103/PhysRevApplied.7.064009

I. INTRODUCTION

After the synthesis of graphene [1] and the discovery of its unique electronic, optical, and thermal properties, research on low-dimensional materials has increased tremendously. Graphene is attractive because of its unique properties, such as its high electronic conductivity and high mobility at room temperature [2–4]. However, its applications are limited in semiconducting devices because of its zero band gap. This gaplessness of graphene has motivated the discovery of alternative nanomaterials that possess a finite band gap and have the potential to replace the silicon in semiconductor technology. Recently, two-dimensional (2D) materials which have a finite band gap, such as monolayers of hexagonal boron nitride [5], transition-metal chalcogenides (MoS_2, WS_2 etc.) [6,7], and phosphorene, have been successfully synthesized [8].

Quasi–one-dimensional materials such as nanoribbons, nanotubes, nanorods, and nanowires have also attracted attention because of their interesting photochemical, photophysical, and transport properties [9,10]. Nanoribbons (NRs) in particular have received great attention from researchers because of their unique electronic properties, which can be modified on the basis of their edge configurations and widths. Quantum confinement because of the presence of edges and their different possible passivations lead to interesting optical, electronic, and magnetic properties. Graphene nanoribbons (GNRs) and boron nitride (BN) nanoribbons have been experimentally synthesized by the unwrapping of carbon nanotubes and BN nanotubes, respectively [11,12]. Armchair GNRs are nonmagnetic semiconductors for all widths, and they have oscillating band gaps over families, approaching the zero band gap of a 2D sheet, for large widths [13]. Zigzag GNRs (ZGNRs), on the other hand, have tunable band gaps ranging from metal to semiconductor, depending on the width and passivation edges [14,15]. Furthermore, ZGNRs also exhibit half-metallic behavior with spin-polarized band gaps when an electric field is applied along the direction of the width of the ribbons, and their gaps can be controlled by the strength of the electric field [16].

C and Si have the same number of electrons; therefore, SiC structures are stable in bulk and have electronic properties which are intermediate between bulk Si and carbon structures. Silicon carbide (SiC) crystallizes in several forms, such as hexagonal, rhombohedral, and cubic Bravais lattices [17]. Bulk SiC is a wide-band-gap semiconductor, and it has been used in high-temperature, high-pressure, and high-frequency device applications [18,19]. The graphenelike 2D SiC monolayer has not been experimentally fabricated yet, but it has been extensively studied using theoretical methods [20–29]. Unlike graphene, it is a direct band-gap semiconductor with a band gap of

*Present address: Physics Department, Bennett University, Plot No. 8-11, TechZone II, Greater Noida 201310, Uttar Pradesh, India.
shukla@phy.iitb.ac.in

2.5 eV. An ultrathin SiC nanosheet which has a thickness of 0.5–1.5 nm has been fabricated, and is used in light-emitting applications [30]. Various SiC structures, such as SiC nanotubes, SiC nanowires, microribbons, and crystalline and bicrystalline nanobelts have also been successfully synthesized [31–34]. Furthermore, multilayer SiC nanoribbons that are micrometers in length and nanometers in thickness have also been synthesized [35].

As far as theory is concerned, SiC nanoribbons have been extensively studied using first-principles calculations, based on the density-functional-theory (DFT) approach [17,21,22,36–43]. Sun *et al.* [21] reported that hydrogen-passivated armchair SiCNRs (ASiCNRs) are direct band-gap semiconductors, with band gaps in the range 2.3–2.4 eV. Furthermore, they reported that band gaps of zigzag SiCNRs (ZSiCNRs) are spin polarized and exhibit intrinsic half-metallic behavior, without the application of an external electric field [21]. Lou and Lee [36] studied narrow ZSiCNRs with widths in the range 0.6–1.6 nm, and they showed that the ferrimagnetic state is more stable, with an antiparallel spin orientation between the two edges. ZSiCNRs that have a half-bare edge were studied by Tang *et al.* [42] using a hybrid DFT approach. They reported that half-bare-edge ZSiCNRs with a bare carbon edge are magnetic semiconductors, while the ones with bare Si edge atoms are magnetic metals. The influence of doping with B and N impurities was studied by Costa and Morbec [41], who showed that B-doped ZSiCNRs retain half-metallic behavior, while N-doped ZSiCNRs become metallic. Lopez-Benzanilla *et al.* [39] employed a local spin-density approximation approach to study sulfur- and oxygen-passivated ZSiCNRs to discover that ZSiCNRs turned from half-metallic to semiconductors, or metals, as a result of passivation. The effects of the substitution of edge atoms, with B and N atoms, was studied by Zheng *et al.* [40], who reported that modified ZSiCNRs are semiconductors. Bekaroglu *et al.* [22] and Morbec and Rahman [43] studied the effects of vacancies on the electronic structure of ZSiCNRs by using the DFT–generalized gradient approximation (GGA) approach, and they found that double (Si and C) vacancies induce magnetism. Ultranarrow ZSiCNRs, including short-range exact-exchange effects, were studied by Lou [44], who obtained lower edge energies and higher band gaps than for those computed using the GGA.

It is well known that the DFT-based approaches underestimate the band gap in semiconductors because they do not include electron-correlation effects [45]. It has been demonstrated that, in nanoribbons, not including correlation effects causes severe errors in comparison to their bulk counterpart because, in low-dimensional systems, these effects are enhanced [46–52]. It will also be interesting to study many-body electron-electron interactions in evaluating accurate band gaps and electron-hole effects in order to calculate optical absorption spectra in ZSiCNRs; this knowledge will enable the exploration of their potential in optical-device applications. In this work, we calculate the quasiparticle band structures and the optical absorption spectra of ZSiCNRs by using the *GW* approximation and solving the Bethe-Salpeter equation (BSE), respectively. We find that ultranarrow ZSiCNRs, with widths narrower than 1 nm, are nonmagnetic semiconductors. *GW* corrections open up significant band gaps in ZSiCNRs that are wider than 1 nm and transform them from half metals to semiconductors. We find that the narrowest ZSiCNR, with a width of 0.6 nm, has strongly bound excitons, with a binding energy of 2.1 eV, while other nanoribbons have weakly bound excitons because their band gaps are too small. Therefore, the narrowest ribbon can be utilized in optoelectronic applications in the infrared frequency range. Broader nanoribbons exhibit distinct band gaps for the two spin orientations, and, therefore, they can be utilized in spintronic devices such as spin valves.

The remainder of this paper is organized as follows. Section II presents details of computations employed in this work, while Sec. III presents the results of our calculations on ZSiCNRs of varying widths. Finally, in Sec. IV, we present our conclusions.

II. COMPUTATIONAL DETAILS

We carry out first-principles many-body electronic-structure calculations for ZSiCNRs using a three-step procedure. First, the DFT calculations are performed using a plane-wave approach, in the GGA [53], with Perdew-Burke-Ernzerhof pseudopotentials [54]. Geometry optimizations are carried out using the computer program Vienna *ab initio* simulation package (VASP) [55]. All of the nanoribbons considered here are fully relaxed until the force on each atom is lower than 0.01 eV/Å. The threshold-energy convergence is set to 10^{-4} eV. A Monokhorst k-point grid of $1 \times 1 \times 11$ is used for Brillouin-zone integration during the relaxation. After the relaxation, we use optimized atomic positions and lattice parameters to calculate Kohn-Sham band gaps of ZSiCNRs using the DFT-GGA approach as implemented in the software package ABINIT [56,57]. GGA wave functions are a good starting point for the many-body calculations, aimed at including electron-correlation effects.

In the second step, we calculate quasiparticle corrections for the DFT-GGA band gaps using the many-body approach G_0W_0 approximation [58], which is a single-shot *GW* approach for computing self-energy corrections in terms of the Green's function (G) and the screened Coulomb potential (W). The screening effects are included by using the plasmon-pole model [59]. A kinetic energy cutoff of 26 hartree is used for all of the systems considered here. Cutoff energies of 5 and 12 hartree are used for the correlation and exchange parts of the self-energy calculations, respectively. A total number of 200 bands are used, out of which more than 120 are unoccupied. In the last step,

the BSE is solved within the Tamm-Dancoff approximation [60] in order to obtain the optical response inclusive of the contribution of the electron-hole interactions, retaining only the resonant part of the Bethe-Salpeter Hamiltonian: This is because the inclusion of the coupling has been shown to have a negligible effect. This approximation has also been used to study similar systems, such as graphene nanoribbons [46,61] and boron nitride nanoribbons [49]. In the *GW* and BSE calculations, a Coulomb truncation scheme is also used to avoid the inclusion of long-range interactions between the periodic images. A $1 \times 1 \times 30$ k-point grid is used in the *GW* and BSE calculations for the systems considered here. Five valence bands and five conduction bands are included to obtain the optical absorption spectra. Nanoribbons are considered to be periodic along the z direction, and more than 13-Å-wide vacuum layers are taken in the nonperiodic directions (the x and y directions) in order to represent an isolated system. The width of a given ZSiCNR is specified by prefixing it with the number of zigzag lines (N_z) across its width. Thus, ZSiCNR-3 denotes a ribbon with $N_z = 3$ zigzag lines across the width. In this work, we study ribbons with $2 \leq N_z \leq 8$, which corresponds to widths between 0.6 and 2.2 nm.

III. RESULTS AND DISCUSSION

A. Formation energy and stability

Figure 1(a) shows the geometric structure of ZSiCNR-4. Optimized bond lengths corresponding to Si—C, Si—H, and C—H are obtained to be 1.77, 1.49, and 1.09 Å, respectively, while the lattice constant is found to be 3.11 Å for all the structures considered here. These parameters are in good agreement with previous studies [21,44]. Here, we calculate the edge formation energies of these nanoribbons in order to understand their thermodynamic stability during edge formation. We evaluate the formation energy by using the following formula:

$$E_f = (E_T - N_{\mathrm{SiC}} E_{\mathrm{SiC}} - 0.5 N_{\mathrm{H}} E_{\mathrm{H_2}})/2l,$$

where E_T is the total energy of the hydrogen-passivated zigzag SiC nanoribbon, E_{SiC} is the total energy of the 2D SiC sheet, $E_{\mathrm{H_2}}$ is the total energy of an isolated hydrogen molecule, N_{SiC} is the number of SiC dimers in the unit cell, N_{H} is the number of H atoms in the unit cell, and l is the periodic length of an edge. In general, the lower the value of E_f of a material, the higher its stability. The formation energy of the ZSiCNRs as a function of width is plotted in Fig. 1(c). Unlike ASiCNRs [52], formation energy of these nanoribbons is strongly dependent on their width, and it increases with the width of the nanoribbons. From the figure, it is obvious that ribbons which have narrow widths have high stability, suggesting that they will be relatively easy to synthesize in the laboratory.

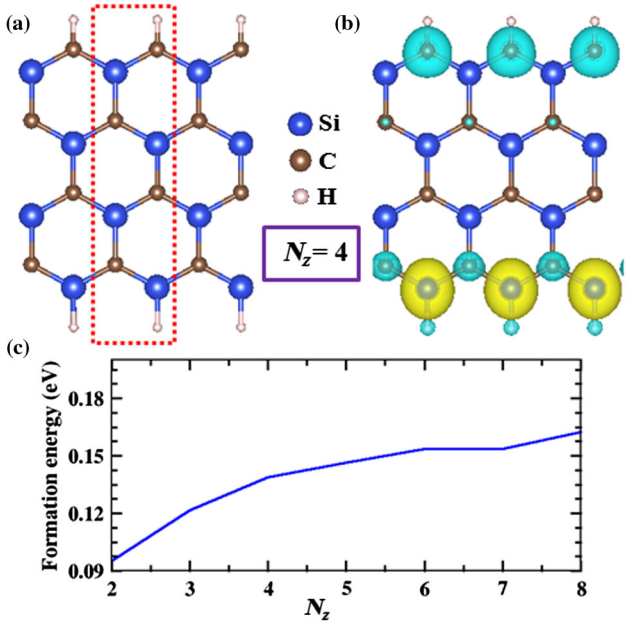

FIG. 1. (a) The geometric structure of a ZSiCNR-4 unit cell shown in the red dashed box is considered for the calculation. (b) The calculated spin density of ZSiCNR-4. Blue and yellow colored spin densities denote opposite spin orientations. (c) The computed edge formation energy of ZSiCNRs as a function of width.

B. Nonmagnetic ZSiCNRs

1. Quasiparticle energies

First, we discuss the electronic structure of ZSiCNRs with widths $N_z = 2$ and 3, which do not exhibit any magnetic behavior. Lou [44] reported that these two nanoribbons are nonmagnetic semiconductors which do not exhibit half-metallic behavior within the GGA or Heyd-Scuseria-Ernzerhof approaches, unlike ribbons which are wider than 1 nm. Their DFT-GGA study predicted that ZSiCNR-2 would be a nonmagnetic semiconductor with a band gap of 0.97 eV, and ZSiCNR-3 is essentially metallic with a band gap of 0.07 eV. Our calculated DFT-GGA and *GW* band structures of ZSiCNR-2 and ZSiCNR-3 are shown in Figs. 2(a) and 2(b), respectively. The blue lines correspond to the DFT GGA, while the red lines denote the *GW* band structure. Our DFT results agree with those of Lou [44]. Figure 2(a) shows that ZSiCNR-2 is a direct band-gap material at the DFT-GGA level, and the gap occurs at the Z point located at the edge of the Brillioun zone. After including the many-body effects, the computed band structure is depicted by the red lines. We find that quasiparticle corrections increase the band gap from 0.97 to 2.4 eV, which is an indirect one (quasidirect) at the *GW* level. In the *GW* band structure of ZSiCNR-2, the valence-band maximum (VBM) occurs a small distance from the Z point, and there is no change in the conduction-band minimum (CBM). Figure 2(b) shows the band structures

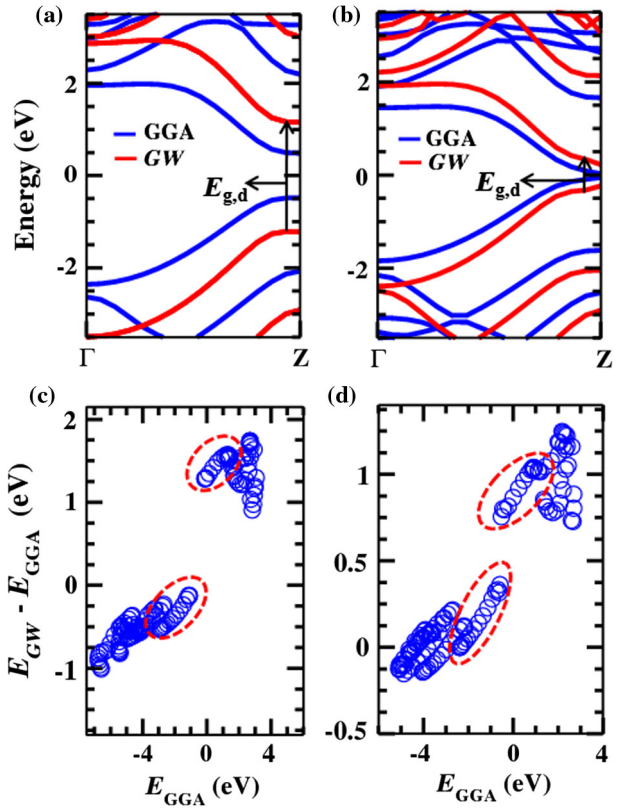

FIG. 2. (a), (b) GGA and *GW* band structures of ZSiCNR-2 and ZSiCNR-3. The blue and red lines represent GGA and *GW* band structures, respectively, and the black arrows denote interband transitions. (c), (d) Quasiparticle self-energy corrections (differences between quasiparticle energies and GGA energy values) for various bands to the GGA Kohn-Sham energies for ZSiCNR-2 and ZSiCNR-3, respectively. Corrections to the states corresponding to the edge atoms in valence and conduction bands are enclosed in the red dashed ellipses.

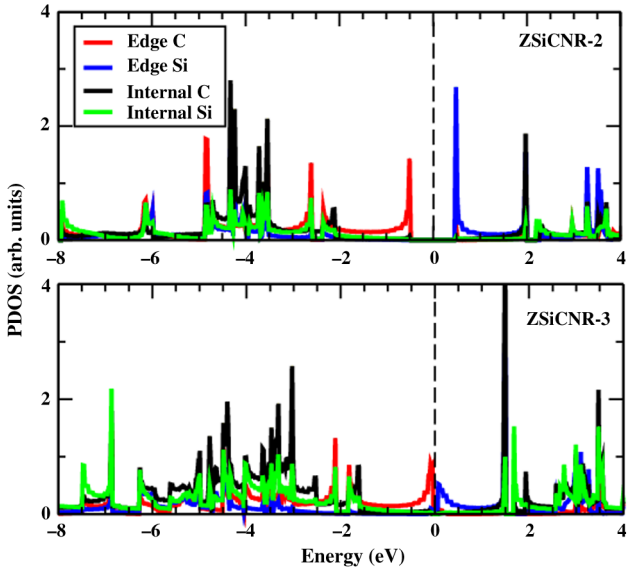

FIG. 3. Projected densities of states for ZSiCNR-2 and ZSiCNR-3. The red and blue curves show states which derive contributions from the edge C and Si atoms, while black and green curves represent states which derive main contributions from internal C and Si atoms, respectively. The Fermi level is represented by the black dashed line, which has been set to 0 eV.

computed by the GGA and *GW* approaches for ZSiCNR-3. Self-energy corrections widen the band gap from 0.07 to 0.45 eV, which is a sixfold increase due to electron-correlation effects. This increase shows that many-body corrections transform ZSiCNR-3 from a nearly metallic system to a semiconductor.

Self-energy corrections for various bands for both of the ribbons are shown in Figs. 2(c) and 2(d). In these nanoribbons, π band states corresponding to the p_x orbital extend into the vacuum perpendicular to the ribbon plane, while the σ states are composed of p_z and p_y orbitals lying in the plane of the sheet. The self-energy corrections to the π states are larger than those to the σ states because of the screening effects due to other π electrons. The corrections enclosed in the red ellipses correspond to the edge states which experience enhanced Coulombic interactions. When compared to the GGA band structure, *GW* bands not only shift but also stretch, by an average of 20%–30%, because of nonuniform quasiparticle corrections. We find that corrections to the states which derive a main contribution from the interior atoms are less linear when compared to states which are predominantly localized on edge atoms.

We present projected densities of states (PDOSs) for ZSiCNR-2 and ZSiCNR-3 in Fig. 3 in order to illustrate the contribution of various atoms from the edges—and the interior—to different orbitals. PDOS plots show that the VBMs in both ribbons arise from edge carbon atoms, while the CBMs are derived from edge Si atoms. The states located on internal C and Si atoms are away from the Fermi level in both ribbons.

2. Optical absorption spectra

Using the quasiparticle band structure, we calculate the optical absorption spectrum of ZSiCNR-2 and ZSiCNR-3 with and without electron-hole interactions, as shown in Figs. 4(a) and 4(b). Electron-hole interactions are incorporated by using the BSE, and in all of the calculations the polarization direction of incident light is considered to be along the length of the nanoribbons. We use the notation $E_{g,d}$ to label the direct transitions which occur between the first valence band and the first conduction band, as shown in Fig. 2. The blue curve represents absorption due to interband transitions at the *GW*-RPA level, while the red curve is a result of solving the BSE, including electron-hole effects. In both ribbons, the first prominent peak comes from the transition between the first valence band and the first conduction band. In *GW*-RPA absorption spectra, we can observe that there are several peaks due to different interband transitions in ZSiCNR-2. However, there is only one prominent peak in ZSiCNR-3, which is a result

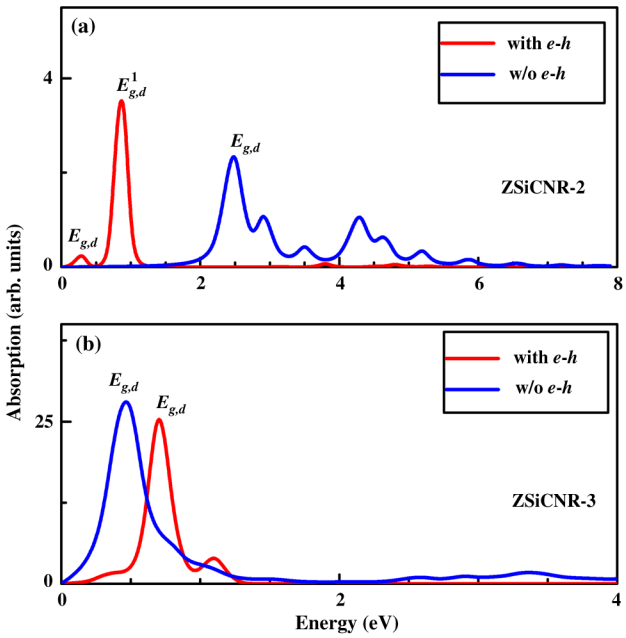

FIG. 4. Optical absorption spectra of (a) ZSiCNR-2 and (b) ZSiCNR-3. The blue curve shows the spectrum computed without the contribution of electron-hole interactions, while the red curve represents the spectrum calculated by including electron-hole interactions.

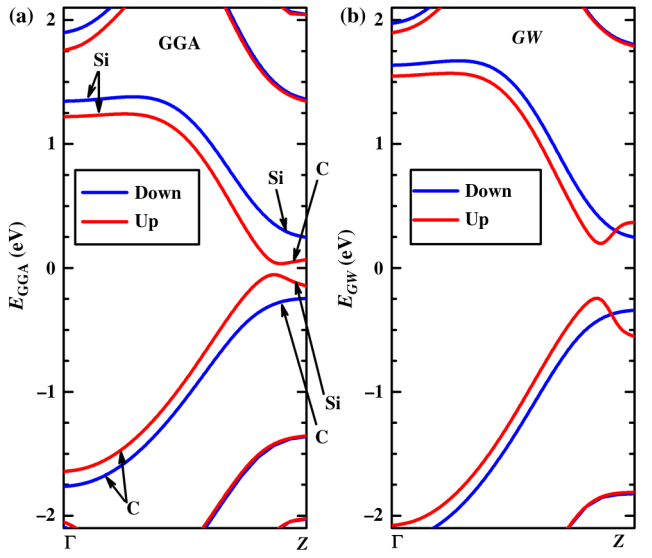

FIG. 5. (a) GGA and (b) quasiparticle band structures of ZSiCNR-4. The red and blue lines represent spin-up and spin-down states, respectively. The atoms contributing to the states of the valence and conduction band on either side of the band gap are marked for ZSiCNR-4. Towards the zone boundary, the states are localized at the ribbon edges.

of the transition between the VBM and the CBM. The inclusion of electron-hole interactions changes the spectrum significantly because not only are the positions of the peaks shifted, but also their shape looks different when compared with the *GW*-RPA absorption spectrum. In the absorption spectra of both the ribbons, which include electron-hole interactions, we observe only one intense excitonic peak due to the transition between the first valence and the first conduction band, $E_{g,d}$. We do not find any other transitions among other bands, even though we include five valence and five conduction bands in our calculations. In Fig. 4, it is obvious that ZSiCNR-2 has a strongly bound exciton, with a binding energy of 2.1 eV ($E_{g,d}$) but a relatively weaker intensity, corresponding to the first absorption peak. We also observe another strongly bound excitonic peak ($E^1_{g,d}$), with a very high intensity and a binding energy of 1.5 eV, originating at distinct k points compared to the first one. These binding energies are significantly larger than the calculated exciton binding energy, 1.17 eV, for the 2D SiC sheet [25], suggesting that the reduced dimensionality and quantum confinement lead to an enhancement in the exciton binding energies of nanoribbons. From among all the ribbons considered here, it is clear that ZSiCNR-2 is a small-gap semiconductor which can be used in optical applications in the low-energy region of the spectrum. Unlike ZSiCNR-2, strongly bound excitons are not observed in ZSiCNR-3 because the band gap is much smaller for this ribbon. The band-to-band absorption-spectrum peak at *GW* level gets blueshifted upon the inclusion of electron-hole effects, as shown in Fig. 4. The final location of the blueshifted absorption peak clearly implies negative exciton binding energy. Thus, the nature of optical transitions contributing to various peaks is also modified in ZSiCNR-3 once the many-body effects are included.

C. Spin-polarized ZSiCNRs

Next, we present the results of quasiparticle-band-structure calculations of spin-polarized ZSiCNR-4 because $N_z = 4$ to $N_z = 8$ have similar band structures and, at mean-field DFT level, exhibit intrinsic half-metallic behavior [21,36]. In Figs. 5(a) and 5(b), we compare the GGA and *GW* quasiparticle band structures of ZSiCNR-4, and we show the widened quasiparticle band gap when electron-correlation effects are included. While the DFT GGA

TABLE I. The values of GGA and *GW* band gaps, and their difference, for spin-polarized ZSiCNRs for widths $N_z = 4$ to 8. Columns 2–4 (columns 5–7) correspond to the spin-up (spin-down) channel. All energies are in eV.

	Spin-up			Spin-down		
N_z	E^{gap}_{GGA}	E^{gap}_{GW}	ΔE^{gap}	$E^{gap}_{2\ GGA}$	E^{gap}_{2GW}	ΔE^{gap}_2
4	0.03	0.33	0.30	0.55	0.59	0.04
5	0.06	0.82	0.76	0.72	0.77	0.05
6	0.006	0.38	0.37	0.64	0.74	0.1
7	0.002	0.384	0.38	0.64	0.92	0.28
8	0.08	0.77	0.69	0.76	0.93	0.14

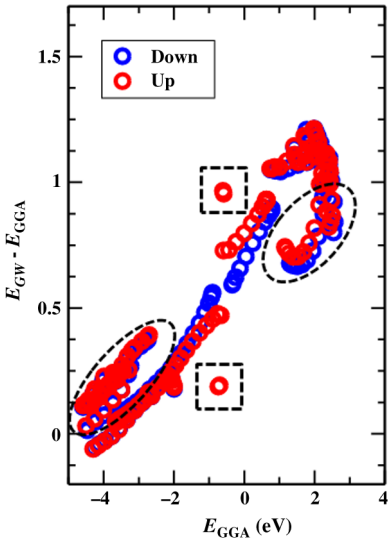

FIG. 6. Quasiparticle–self-energy corrections to the GGA–Kohn-Sham energies of ZSiCNR-4. The blue and red empty circles represent spin-up and spin-down states, respectively. Corrections to the spin-up edge states are shown in the dashed rectangular boxes. The dashed ellipses enclose the σ states.

predicts a very small gap of 30 meV, the *GW* quasiparticle gap is seen to have widened to 0.33 eV, clearly showing that the ZSiCNRs are narrow-gap semiconductors (Table I). Although, half-metallicity disappears after the inclusion of many-body effects through *GW* calculations, the band gaps for the two spin orientations remain different. The atoms contributing to various states are marked in Fig. 5(a). Towards the zone boundary, the states of the first valence and conduction bands of both spins are localized at the ribbon edges [36]. From the spin-density plot presented in Fig. 1(b), it is obvious that the spins localized on the two edges have opposing spin orientations. The states to the left of the VBM or CBM extend over the entire ribbon width, except for the spin-down conduction band, which mainly comprises of the Si edge states. The screening at the edges shows a complicated dependence on the states, which is enhanced in ZSiCNRs because the charge and spin distributions differ at the Si and C edges. Figure 6 shows that the self-energy corrections are highly state dependent. The states which are enclosed in rectangular boxes away from the main region represent the spin-up edge states (valence states at the Si edge and conduction states at the C edge). As the wave vector approaches the zone boundary (the *Z* point), the states get more localized at the edges [62], and the deviations between the up- and down-spin states, as also the energy gap for the up-spin states, become larger [cf. Fig. 5(a)]. Thus, the nature of spin-up bands is very similar to the bands in spin-degenerate zigzag graphene nanoribbons [48].

The larger spin-down gap at the zone boundary exhibits a smaller quasiparticle correction. Figure 6 shows the valence spin-down states bending away from the spin-up states, and, similarly, that the spin-down states of the conduction band also have smaller corrections than the corresponding spin-up states. These states correspond to the valence C and the conduction Si states localized at the edges. The spin-down edge states show smaller self-energy corrections than those localized in the interior, while the spin-up edge states exhibit exactly the opposite behavior. The charge distributions are different at the two edges, leading to varying amounts of screening. For example, in the ground state, there is a partial valence electron transfer from Si to C [63]. As a consequence, the edge C states are screened more and have smaller self-energy corrections, while the lesser screened edge valence Si states experience enhanced Coulomb interactions. Therefore, the spin-down band gap does not change as much as the spin-up band gap.

A few of the points enclosed by dashed circles lying outside the main region are σ states. Apart from the first valence and conduction bands, the next few bands comprise both σ and π states (shown in Fig. 6). Similar to ASiCNRs [52] and narrow ZSiCNRs, the σ states have smaller self-energy corrections than the π states.

For the sake of completeness, we also perform calculations on the nonmagnetic (i.e., non-spin-polarized) states of the ZSiCNRs, and we find that a spin-polarized state does not exist for narrow ribbons ($N_z = 2, 3$), and spin-polarized calculations for those ribbons yield the same results as nonmagnetic calculations. However, for broader ribbons, both spin-polarized and nonmagnetic states exist and, quite expectedly, the total energies for the spin-polarized cases are lower than for the nonmagnetic ones (see Table II). We also perform GGA and *GW* calculations for the nonmagnetic states of broader ribbons, and the results are presented in

TABLE II. Total energies per unit cell for nonmagnetic (NM) and spin-polarized (SP) ZSiCNRs for widths $N_z = 4$ to 6. The last column gives the energy difference between the two configurations.

	Total energy (eV)		
N_z	NM	SP	ΔE (eV)
4	−62.106 675	−62.115 140	0.008 465
5	−76.101 117	−76.120 842	0.019 725
6	−90.119 364	−90.144 896	0.025 532

TABLE III. The values of the GGA and *GW* band gaps—and their difference—for nonmagnetic states of ZSiCNRs with widths $N_z = 2$ to 6. All of the energy values are in eV.

N_z	E_{GGA}^{gap}	E_{GW}^{gap}	ΔE^{gap}
2	0.97	2.4	1.43
3	0.07	0.45	0.36
4	0.011	0.22	0.209
5	0.015	0.15	0.135
6	0.002	0.07	0.068

Table III. From the table, it is obvious that (a) at DFT-GGA level, band gaps of the ribbons decrease rapidly with their width, and (b) quasiparticle corrections are large for the ultranarrow ZSiCNRs, but they also reduce in magnitude rapidly with increasing width. Combining these two results, we conclude that nonmagnetic calculations predict that broader ZSiCNRs will exhibit metallic behavior. Therefore, an experimental measurement of the band gaps of broader ZSiCNRs can settle the issue regarding whether these systems exhibit a magnetic ground state or a nonmagnetic one.

We have not presented optical absorption spectra of spin-polarized ZSiCNRs, as they undergo different quasiparticle–self-energy corrections because of two spin band gaps. We can expect weakly bound excitons in ribbons that are wider than 1 nm. The small band gap of ZSiCNRs which are wider than 0.6 nm makes them potentially useful in IR devices.

IV. CONCLUSIONS

In this paper, we perform first-principles many-body calculations in order to investigate quasiparticle band structures and optical absorption of hydrogen-passivated zigzag SiC nanoribbons with widths ranging from 0.6 to 2.2 nm. For the study, a computationally intensive *GW* approximation is employed to compute the self-energy–corrected quasiparticle band gaps. We also use the BSE to calculate optical absorption spectra including electron-hole effects. It is found that the many-body effects are significant due to the reduced dimensionality of nanoribbons. Self-energy corrections transform nearly half-metallic zigzag SiC nanoribbons with widths larger than 1 nm to semiconductors. The inclusion of electron-hole effects changes optical absorption spectra in a significant manner, both qualitatively and quantitatively. The excitonic binding energies and luminescence properties are dependent on the width of the ribbon. We find that a nanoribbon with a width of 0.6 nm has strongly bound excitons with a binding energy of 2.1 eV, suggesting its possible utility in optoelectronic applications. We also compute the edge formation energy and show that narrower ribbons are more stable than wider ones. The unique Coulombic interactions at the spin-polarized edges make zigzag SiC nanoribbons interesting systems to study. As far as the behavior of their band gaps with respect to width is concerned, because the band gaps in half-metallic ZSiCNRs arise due to the presence of magnetic edge states, broader ribbons are therefore expected to have spin-polarized nonzero band gaps, hinting at their possible utility in spintronic applications, such as with spin valves.

ACKNOWLEDGMENTS

N. A. and N. M. gratefully acknowledge the support from Monash HPC, the National Computing Infrastructure of Australia, and the Pawsey Supercomputing facility. This research was partially supported by the Australian Research Council Centre of Excellence in Future Low-Energy Electronics Technologies (Project No. CE170100039) and funded by the Australian Government. A. S. acknowledges the financial support from the Department of Science and Technology, Government of India under Project No. SB/S2/CMP-066/2013.

[1] K. S. Novoselov, A. K. Geim, S. V. Morozov, D. Jiang, Y. Zhang, S. V. Dubonos, I. V. Grigorieva, and A. A. Firsov, Electric field effect in atomically thin carbon films, Science **306**, 666 (2004).

[2] Andre K. Geim and Konstantin S. Novoselov, The rise of graphene, Nat. Mater. **6**, 183 (2007).

[3] Mikhail I. Katsnelson, Graphene: Carbon in two dimensions, Mater. Today **10**, 20 (2007).

[4] A. H. Castro Neto, F. Guinea, N. M. R. Peres, K. S. Novoselov, and A. K. Geim, The electronic properties of graphene, Rev. Mod. Phys. **81**, 109 (2009).

[5] Jonathan N. Coleman, Mustafa Lotya, Arlene O'Neill, Shane D. Bergin, Paul J. King, Umar Khan, Karen Young, Alexandre Gaucher, Sukanta De, Ronan J. Smith *et al.*, Two-dimensional nanosheets produced by liquid exfoliation of layered materials, Science **331**, 568 (2011).

[6] Kin Fai Mak, Changgu Lee, James Hone, Jie Shan, and Tony F. Heinz, Atomically Thin MoS_2: A New Direct-Gap Semiconductor, Phys. Rev. Lett. **105**, 136805 (2010).

[7] Qing Hua Wang, Kourosh Kalantar-Zadeh, Andras Kis, Jonathan N. Coleman, and Michael S. Strano, Electronics and optoelectronics of two-dimensional transition metal dichalcogenides, Nat. Nanotechnol. **7**, 699 (2012).

[8] Han Liu, Adam T. Neal, Zhen Zhu, Zhe Luo, Xianfan Xu, David Tománek, and Peide D. Ye, Phosphorene: An unexplored 2D semiconductor with a high hole mobility, ACS Nano **8**, 4033 (2014).

[9] Y. Xia, P. Yang, Y. Sun, Y. Wu, B. Mayers, B. Gates, Y. Yin, F. Kim, and H. Yan, One-dimensional nanostructures: Synthesis, characterization, and applications, Adv. Mater. **15**, 353 (2003).

[10] Xun Wang and Yadong Li, Solution-based synthetic strategies for 1-D nanostructures, Inorg. Chem. **45**, 7522 (2006).

[11] Dmitry V. Kosynkin, Amanda L. Higginbotham, Alexander Sinitskii, Jay R. Lomeda, Ayrat Dimiev, B. Katherine Price, and James M. Tour, Longitudinal unzipping of carbon nanotubes to form graphene nanoribbons, Nature (London) **458**, 872 (2009).

[12] Haibo Zeng, Chunyi Zhi, Zhuhua Zhang, Xianlong Wei, Xuebin Wang, Wanlin Guo, Yoshio Bando, and Dmitri Golberg, White graphenes,: Boron nitride nanoribbons via boron nitride nanotube unwrapping, Nano Lett. **10**, 5049 (2010).

[13] Young-Woo Son, Marvin L. Cohen, and Steven G. Louie, Energy Gaps in Graphene Nanoribbons, Phys. Rev. Lett. **97**, 216803 (2006).

[14] Ashwin Ramasubramaniam, Electronic structure of oxygen-terminated zigzag graphene nanoribbons: A hybrid density functional theory study, Phys. Rev. B **81**, 245413 (2010).

[15] Geunsik Lee and Kyeongjae Cho, Electronic structures of zigzag graphene nanoribbons with edge hydrogenation and oxidation, Phys. Rev. B **79**, 165440 (2009).
[16] Young-Woo Son, Marvin L. Cohen, and Steven G. Louie, Half-metallic graphene nanoribbons, Nature (London) **444**, 347 (2006).
[17] Ping Lou, Effects of edge hydrogenation in zigzag silicon carbide nanoribbons: Stability, electronic and magnetic properties, as well as spin transport property, J. Mater. Chem. C **1**, 2996 (2013).
[18] Garry L. Harris, *Properties of Silicon Carbide*, 1st ed. (Institution of Electrical Engineers, London, 1995).
[19] P. A. Ivanov and V. E. Chelnokov, Recent developments in SiC single-crystal electronics, Semicond. Sci. Technol. **7**, 863 (1992).
[20] Xiao Lin, Shisheng Lin, Yang Xu, Ayaz Ali Hakro, Tawfique Hasan, Baile Zhang, Bin Yu, Jikui Luo, Erping Li, and Hongsheng Chen, *Ab initio* study of electronic and optical behavior of two-dimensional silicon carbide, J. Mater. Chem. C **1**, 2131 (2013).
[21] Lian Sun, Yafei Li, Zhenyu Li, Qunxiang Li, Zhen Zhou, Zhongfang Chen, Jinlong Yang, and J. G. Hou, Electronic structures of SiC nanoribbons, J. Chem. Phys. **129**, 174114 (2008).
[22] E. Bekaroglu, M. Topsakal, S. Cahangirov, and S. Ciraci, First-principles study of defects and adatoms in silicon carbide honeycomb structures, Phys. Rev. B **81**, 075433 (2010).
[23] Tie-Yu Lu, Xia-Xia Liao, Hui-Qiong Wang, and Jin-Cheng Zheng, Tuning the indirect-direct band gap transition of SiC, GeC and SnC monolayer in a graphene-like honeycomb structure by strain engineering: A quasiparticle *GW* study, J. Mater. Chem. **22**, 10062 (2012).
[24] Yi Ding and Yanli Wang, Density functional theory study of the silicene-like SiX and XSi_3 (X = B, C, N, Al, P) honeycomb lattices: The various buckled structures and versatile electronic properties, J. Phys. Chem. C **117**, 18266 (2013).
[25] H. C. Hsueh, G. Y. Guo, and Steven G. Louie, Excitonic effects in the optical properties of a SiC sheet and nanotubes, Phys. Rev. B **84**, 085404 (2011).
[26] Björn Baumeier, Peter Krüger, and Johannes Pollmann, Structural, elastic, and electronic properties of SiC, BN, and BeO nanotubes, Phys. Rev. B **76**, 085407 (2007).
[27] H.Şahin, S. Cahangirov, M. Topsakal, E. Bekaroglu, E. Akturk, R. T. Senger, and S. Ciraci, Monolayer honeycomb structures of group-IV elements and III–V binary compounds: First-principles calculations, Phys. Rev. B **80**, 155453 (2009).
[28] I. J. Wu and G. Y. Guo, Optical properties of SiC nanotubes: An *ab initio* study, Phys. Rev. B **76**, 035343 (2007).
[29] Kun Zhao, Mingwen Zhao, Zhenhai Wang, and Yingcai Fan, Tight-binding model for the electronic structures of SiC and BN nanoribbons, Physica (Amsterdam) **43E**, 440 (2010).
[30] S. S. Lin, Light-emitting two-dimensional ultrathin silicon carbide, J. Phys. Chem. C **116**, 3951 (2012).
[31] Xu-Hui Sun, Chi-Pui Li, Wing-Kwong Wong, Ning-Bew Wong, Chun-Sing Lee, Shuit-Tong Lee, and Boon-Keng Teo, Formation of silicon carbide nanotubes and nanowires via reaction of silicon (from disproportionation of silicon monoxide) with carbon nanotubes, J. Am. Chem. Soc. **124**, 14464 (2002).
[32] Gleb N. Yushin, Z. Goknur Cambaz, Yury Gogotsi, Kateryna L. Vyshnyakova, and Lyudmila N. Pereselentseva, Carbothermal synthesis of α-SiC micro-ribbons, J. Am. Ceram. Soc. **91**, 83 (2008).
[33] Guangcheng Xi, Yiya Peng, Songming Wan, Tanwei Li, Weichao Yu, and Yitai Qian, Lithium-assisted synthesis and characterization of crystalline 3C-SiC nanobelts, J. Phys. Chem. B **108**, 20102 (2004).
[34] Renbing Wu, Lingling Wu, Guangyi Yang, Yi Pan, Jianjun Chen, Rui Zhai, and Jing Lin, Fabrication and photoluminescence of bicrystalline SiC nanobelts, J. Phys. D **40**, 3697 (2007).
[35] Huan Zhang, Weiqiang Ding, Kai He, and Ming Li, Synthesis and characterization of crystalline silicon carbide nanoribbons, Nanoscale Res. Lett. **5**, 1264 (2010).
[36] Ping Lou and Jin Yong Lee, Band structures of narrow zigzag silicon carbon nanoribbons, J. Phys. Chem. C **113**, 12637 (2009).
[37] Ping Lou and Jin Yong Lee, Electrical control of magnetization in narrow zigzag silicon carbon nanoribbons, J. Phys. Chem. C **113**, 21213 (2009).
[38] Yi Ding and Yanli Wang, Electronic structures of zigzag SiC nanoribbons with asymmetric hydrogen-terminations, Appl. Phys. Lett. **101**, 013102 (2012).
[39] Alejandro Lopez-Bezanilla, Jingsong Huang, Paul R. C. Kent, and Bobby G. Sumpter, Tuning from half-metallic to semiconducting behavior in SiC nanoribbons, J. Phys. Chem. C **117**, 15447 (2013).
[40] Fang-Ling Zheng, Yan Zhang, Jian-Min Zhang, and Ke-Wei Xu, Bandgap modulations of silicon carbon nanoribbons by transverse electric fields: A theoretical study, Phys. Status Solidi (b) **248**, 1676 (2011).
[41] C. D. Costa and J. M. Morbec, Boron and nitrogen impurities in SiC nanoribbons: An *ab initio* investigation, J. Phys. Condens. Matter **23**, 205504 (2011).
[42] Zhen-Kun Tang, Ling-Ling Wang, Li-Ming Tang, Wei-Qing Huang, Deng-Yu Zhang, Liang Xu, and Xiao-Fei Li, Electronic and magnetism properties of half-bare zigzag silicon carbon nanoribbons from hybrid density functional calculations, Solid State Commun. **158**, 25 (2013).
[43] Juliana M. Morbec and Gul Rahman, Role of vacancies in the magnetic and electronic properties of SiC nanoribbons: An *ab initio* study, Phys. Rev. B **87**, 115428 (2013).
[44] Ping Lou, Short-range exact exchange effects in ultranarrow zigzag silicon carbide nanoribbons, Phys. Status Solidi (b) **251**, 423 (2014).
[45] R. W. Godby, M. Schlüter, and L. J. Sham, Accurate Exchange-Correlation Potential for Silicon and Its Discontinuity on Addition of an Electron, Phys. Rev. Lett. **56**, 2415 (1986).
[46] Deborah Prezzi, Daniele Varsano, Alice Ruini, Andrea Marini, and Elisa Molinari, Optical properties of graphene nanoribbons: The role of many-body effects, Phys. Rev. B **77**, 041404 (2008).
[47] Li Yang, Marvin L. Cohen, and Steven G. Louie, Excitonic effects in the optical spectra of graphene nanoribbons, Nano Lett. **7**, 3112 (2007).

[48] Li Yang, Marvin L. Cohen, and Steven G. Louie, Magnetic Edge-State Excitons in Zigzag Graphene Nanoribbons, Phys. Rev. Lett. **101**, 186401 (2008).

[49] Shudong Wang, Qian Chen, and Jinlan Wang, Optical properties of boron nitride nanoribbons: Excitonic effects, Appl. Phys. Lett. **99**, 063114 (2011).

[50] Chunping Hu, Ryo Ogura, Nobuhito Onoda, Satoru Konabe, and Kazuyuki Watanabe, Quasiparticle band gaps of boron nitride nanoribbons, Phys. Rev. B **85**, 245420 (2012).

[51] Jongmin Kim, Won Seok Yun, and J. D. Lee, Optical absorption of armchair MoS_2 nanoribbons: Enhanced correlation effects in the reduced dimension, J. Phys. Chem. C **119**, 13901 (2015).

[52] Naresh Alaal, Vaideesh Loganathan, Nikhil Medhekar, and Alok Shukla, First principles many-body calculations of electronic structure and optical properties of SiC nanoribbons, J. Phys. D **49**, 105306 (2016).

[53] Martin Fuchs and Matthias Scheffler, *Ab initio* pseudopotentials for electronic structure calculations of poly-atomic systems using density-functional theory, Comput. Phys. Commun. **119**, 67 (1999).

[54] Martin Fuchs and Matthias Scheffler, *Ab initio* pseudopotentials for electronic structure calculations of poly-atomic systems using density-functional theory, Comput. Phys. Commun. **119**, 67 (1999).

[55] G. Kresse and J. Furthmüller, Efficiency of *ab initio* total energy calculations for metals and semiconductors using a plane-wave basis set, Comput. Mater. Sci. **6**, 15 (1996).

[56] X. Gonze *et al.*, ABINIT: First-principles approach to material and nanosystem properties, Comput. Phys. Commun. **180**, 2582 (2009).

[57] Xavier Gonze, A brief introduction to the ABINIT software package, Z. Kristallogr. **220**, 558 (2005).

[58] Giovanni Onida, Lucia Reining, and Angel Rubio, Electronic excitations: Density-functional versus many-body Green's-function approaches, Rev. Mod. Phys. **74**, 601 (2002).

[59] R. W. Godby and R. J. Needs, Metal-Insulator Transition in Kohn-Sham Theory and Quasiparticle Theory, Phys. Rev. Lett. **62**, 1169 (1989).

[60] Alexander L. Fetter and John D. Walecka, *Quatum Theory of Many-Particle Systems*, 1st ed. (McGraw-Hill, New York, 1971).

[61] Richard Denk, Michael Hohage, Peter Zeppenfeld, Jinming Cai, Carlo A. Pignedoli, Hajo Söde, Roman Fasel, Xinliang Feng, Klaus Müllen, Shudong Wang *et al.*, Exciton-dominated optical response of ultra-narrow graphene nanoribbons, Nat. Commun. **5**, 4253 (2014).

[62] Mitsutaka Fujita, Katsunori Wakabayashi, Kyoko Nakada, and Koichi Kusakabe, Peculiar localized state at zigzag graphite edge, J. Phys. Soc. Jpn. **65**, 1920 (1996).

[63] Jian-Min Zhang, Fang-Ling Zheng, Yan Zhang, and Vincent Ji, First-principles study on electronic properties of SiC nanoribbon, J. Mater. Sci. **45**, 3259 (2010).